# Detector Resolution in Jet Fragmentation

Scott Crawshaw

Supervisor: Peter Skands

# Contents

# 1 Abstract

This project aims to estimate the influence of detector resolutions in measuring QCD jet rates at two proposed future $e^+e^-$ colliders. The primary focus will be assessing the effects of histogram 'bin migration', caused by detector resolution smearing. The smearing analysis focuses on the logarithmic measure of the $k\perp$ Durham clustering algorithm, which is widely used in QCD studies. The bin migration had a counter-intuitive effect, where a finer bin size resulted in lower bin migration. This seems unlikely, and suggests an error has been made in calculating the bin migration matrix.

# 2 Background Theory

Quantum Chromodynamics (QCD) is the theory of the nuclear strong force, which is the fundamental interaction of quarks are gluons. Quarks and gluons cannot be directly detected, as they are 'confined'. These fundamental particles 'hadronize' within a distance of 1 fm, and therefore their properties must be determined indirectly from observing the interactions of high energy particles. The chosen interaction that this project has focused on is the electron positron annihilation at a $\sqrt{s}$ energy of 91.2 GeV. At this centre of mass energy, the electron-positron annihilation results in the production of the Z boson, which quickly decays into a quark anti-quark pair (at leading order). This is shown in Figure 1. The electron-positron annihilation is especially well suited as a reference case that basic parameters of QCD can be determined, because of the 'clean energy distribution' of the quark anti-quark pair. The energy of the partons are determined by the fragmentation function (equation 1 [1]).

$$F^h(x,s) = \Sigma \int_x^1 \frac{dz}{z} g_i(s)\delta(1-z)D_i^h(x/z,s) \tag{1}$$

The presence of the delta function means that the energy distribution of the quarks is precisely determined, resulting in the 'clean energy distribution'. With this information, the parameters of QCD can be determined to a degree of precision not offered in particle collisions with a less certain distribution of energy.

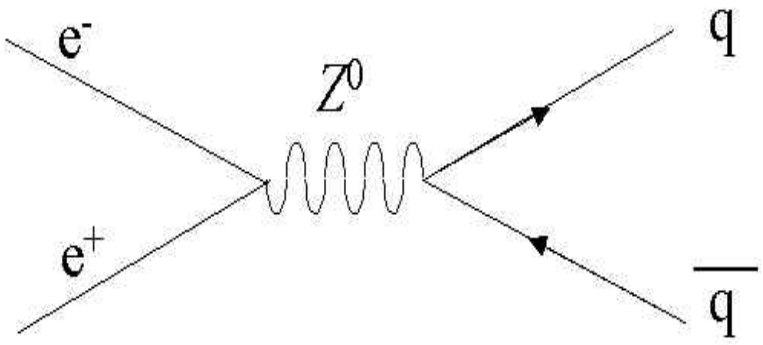


Figure 1: Feynman Diagram representing the leading order electron-positron annhilation.

In this Feynman Diagram, time proceeds from left to right. On the left hand of the diagram, the electron (which has an arrow pointing forward in time) meets and annhilates with the incoming positron (which has an arrow pointing backwards in time). This can produce either a photon, or a Z boson. On the right hand side, a quark anti-quark pair appear. This quark anti-quark pair will quickly hadronise into a number of particles, which will be received by the particle detectors. As the partons (a term used to describe quarks or gluons) race away from the event, they quickly radiate further gluons, and begin to form hadrons. A final state will result in a number of different hadrons, leptons and photons being produced. A simple process with 2 or 3 final state hadrons may have a multitude of intermediary particles partons, before these particles hadronise. As the number of intermediary particles increase, the degrees of freedom rapidly get out of hand.

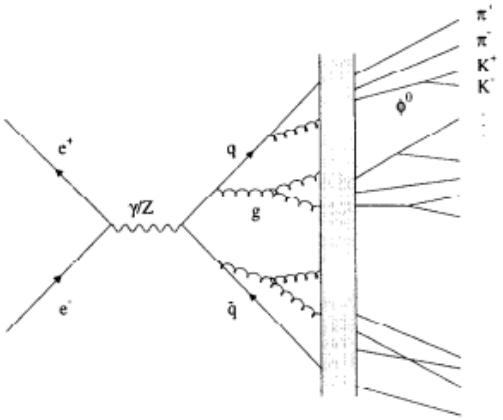


Figure 2: Feynman Diagram of a possible Z boson decay [3]

In this specific example, our final state involves 13 products, which at the very least would involve 39 degrees of freedom, although a four dimensional constraint would reduce this to 35 degrees of freedom. This is without addressing it's particular parton composition of each state. The phase space for multi-dimensional problem rapidly expands as the number of final state particles are produced.

To simplify this problem, theorists use a jet clustering algorithm to simplify the calculations used, and make a mapping of the final state of the hadronisation onto a perturbative expansion of quantum field theory. So if we are to have any understanding at all of sub-hadronic physics, we have to use approximations, and gradually increase the accuracy of our approximation.

In practice, the precision of measurements of the parameters of QCD is limited by our ability to compute the theory of QCD. Fixed order perturbative calculations are only available to finite order (typically no higher than NNLO) and the non-perturbative hadronization aspects aren't fully understood.

An illustration of the jets detected is shown below.

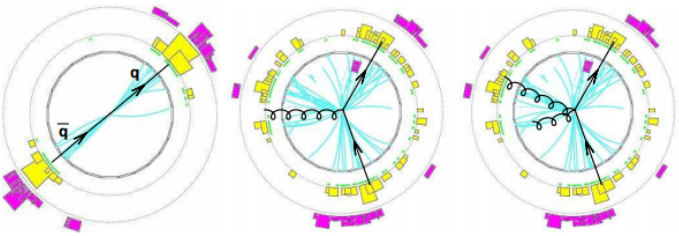


Figure 3: Illustration of possible jets [2]

The figure above shows possible scenarios that could be detected. The left event is a two jet event. The middle event and the right event are considerably more difficult to analyse. This illustrates the need to cluster the jets, so that some leading order, or next to leading order approximation can be used.

The purpose of jet-clustering algorithms is to determine at what resolution scale a three jet event should look like a two jet event, or what energy a four jet event will look like a three jet event etc. This is essentially a mapping of the final state, which is not solvable analytically, to a leading order, or next to leading order approximation.

The most extensive studies Z boson decays from electron positron annhilations was conducted at the Large Electron Positron collider (LEP). This project has compared results from the detector known as ALEPH (A detector for LEP Physics), one of four detectors at LEP. ALEPH was able to record several million hadronic Z decays, but the statistical uncertainty is still of a comparable magnitude to the systematic uncertainty. The largest statistical error from ALEPH was $\pm$ 0.0012 for the probability of finding a particle within a 0.2 $ln(1/y_{23})$ bin. The systematic error for this probability was 0.005. The proposed detectors to be built will have $10^9$ bosons produced (at the ILC) [3], or $10^12$ (at the FCC)

[4]. This means that statistical uncertainties will drop, making the systematic uncertainties the dominant source of error. The most significant components of the detectors are the particle tracking chamber, the Electromagnetic Calorimeter (ECAL), and the Hadronic Calorimeter (HCAL). The diagram below, provided by ALEPH, is an illustration of the detectors around the point where the electrons and positrons annhilate, and the Z boson is produced.

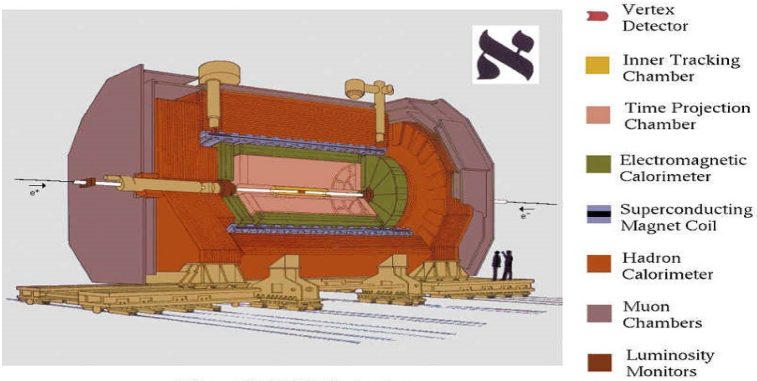


Figure 4: Illustration of ALEPH detector [5]

The particle tracker is the detector that immediately surrounds the beam axis. As the particles move through these trackers, the charged particles will leave pulses on wires within the tracking chamber. The magnetic field in the chamber (approximately 1.5 T)[3] causes the particles to curve. The resultant curvature of the trajectory allow the momentum of the particles to be determined. For particles with lower momentum tend to curve more, as they remain in the tracking chamber longer than their high momentum counterparts. This means that the uncertainty in the measurement of the transverse momentum increases as the particles momentum increases.

An electromagnetic calorimeter is a lead/wire-chamber sampling device. This uses a scintillating crystal material to interact with incoming electrons and photons. This material will release photons when it is struck by incoming electrons or photons. A photo multiplier is then used to detect these produced photons. The intensity of the received signal is proportional to the energy of the incoming particles. To prevent multiple cascades of emitted photons interacting with the material, multiple layers are used. The energy in the system can then be calculated by analysing the information of the tracker, and the energy deposited in the ECAL.

Neither the tracker nor the ECAL stops any hadronic material from passing through. There aren't any nuclear interactions, allowing all of these particles to pass through. The final component is the hadron calorimeter (HCAL). The hadron calorimeter consists of slabs of iron, which collects the hadronic particles. As iron is difficult to take measurements directly from, the slabs of iron are

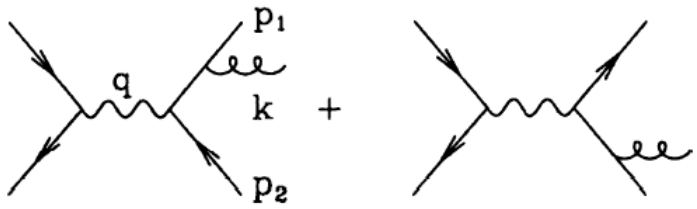


Figure 5: Illustration of ALEPH detector

interspersed with an active material that measurements can be made with. This allows experimentalists a more accurate way to determine the stopping distance of the particles, rather than just having one solid sheet of iron. By creating a new detector with more hadronic decays produced, and increased resolution, the precision of measurements can be increased. This means that the parameters of QCD will be more finely tuned, allowing future experiments a chance to confirm or break current predictions.

The emission of gluons in QCD is very similar to bremsstrahlung radiation of photons in QED. Soft photons that are emitted collinearly to the electron have a greater quantum amplitude, and so are more likely to be observed. To calculate QCD analytically, we can look at Feynman Diagrams. In figure 4, we can see a set of Feynman diagrams.

This represents two possible outcomes at next to leading order for a Z boson decay. The momentum of each particle is described on the left hand diagram, and is completely applicable to the right hand diagram. Using the Feynman rules, and approximating the quarks as massless, the propagator of this vertex is given as:

$$\frac{1}{k^2} = \frac{1}{E_i \cdot E_j \cdot (1 - cos\theta_{ij})} \tag{2}$$

If the denominator on the right hand side of equation 1 approaches zero, the propagator approaches infinity, meaning that the probability for this occurs approaches unity. This means that this reaction is more likely to be observed. This suggests that to cluster the particles into jet, a convenient measure of the jets is to focus on this reaction. This approach to clustering is called the $k_\perp$ Durham algorithm, which is defined as:

$$k_\perp^2 = 2 \cdot min\{E_i^2, E_j^2\} \cdot (1 - cos\theta_{ij}) \tag{3}$$

This algorithm will compare the squared energy of each particle detected in the detector, and take the value of the smallest energy of the pair. If $k_\perp > k_{cutoff}$, the algorithm will identify the pair as two separate jets. If $k_\perp$ is less than the cutoff threshold, the algorithm will set the pair as a new 'pseudo-particle', which has an energy which is the minimum of the pair. The algorithm can then be modified by scaling it with the centre of mass energy.

$$y_{ij} = 2 \cdot \frac{min\{E_i^2, E_j^2\}}{E_{CM}^2} \cdot (1 - cos\theta_{ij}) \tag{4}$$

# 3 Method

As this project aims to determine the accuracy of measurements for future detectors, it is vital to determine how measurement uncertainties propagate to calculated values. To find the uncertainty $u(f)$ in a function $f = f(x, y, z, ...)$, the chain rule is used:

$$u(f) = \sqrt{\left(\frac{\partial f}{\partial x}u(x)\right)^2 + \left(\frac{\partial f}{\partial y}u(y)\right)^2 + \left(\frac{\partial f}{\partial z}u(z)\right)^2 + ...} \tag{5}$$

For the purpose of this analysis, the uncertainty in the angular resolution is considered zero, as the uncertainty in the energy is dominant.

Applying the chain rule to the Durham Algorithm, yields:

$$u(y) = \frac{2y_{ij}}{E} \cdot u(E) \tag{6}$$

As the minimum function is not a continuous function, the chain rule does not apply. To avoid this, a continuous approximation of the minimum function was used. A detailed proof of this is attached in Appendix A.

To determine the error propagation in the logarithm of $\frac{1}{7}y_{ij}$, the chain rule is applied. This gives:

$$u\left(ln(\frac{1}{y_{ij}})\right) = \frac{2 \cdot u(E)}{E} \tag{7}$$

A set of uncertainty values were provided by M. Dams, Niels Bohr Institute, Copenhagen. [6]

The uncertainty of the particle tracker proposed to be used in the new Silicon Detector (Si-DET) is given as:

$$\frac{u(p_T)}{p_T^2} = \sqrt{(2 \times 10^{-5})^2 + (\frac{2 \times 10^{-3}}{p_T})^2} \tag{8}$$

The uncertainty of the particle tracker at ALEPH was stated to be approximately $6 \times 10^{-4}$ when the momentum is 45 GeV. Assuming that the uncertainties of the ALEPH detector assume the behaviour of the new particle tracker, the uncertainty should vary as such:

$$\frac{u(p_T)}{p_T^2} = \sqrt{(2 \times 10^{-5})^2 + (\frac{2.7 \times 10^{-2}}{p_T^2})} \tag{9}$$

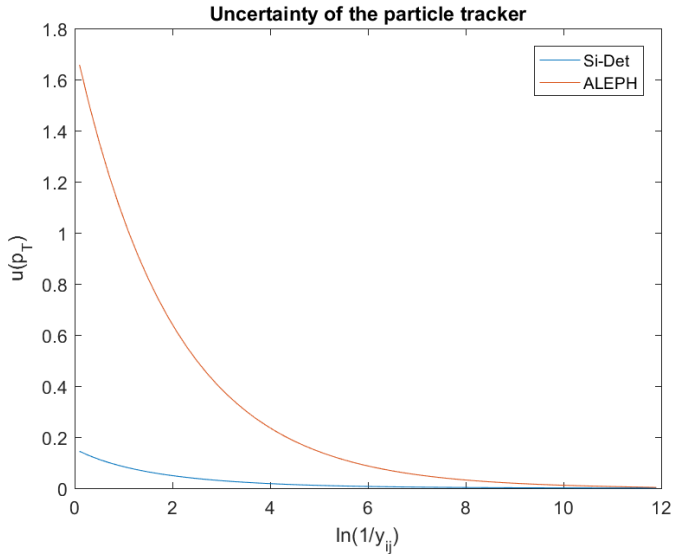


Figure 6: Uncertainty of momentum in the particle tracker

The relationship between momentum and energy is given (in natural units) as:

$$E^2 - p^2 = m^2 \tag{10}$$

A comparison between the ALEPH particle tracker and the Si-DET particle tracker is shown below. As the momentum increases, the energy of the particle increases, which in turn causes $y_{ij}$ to increase. The x axis represents the logarithm of the inverse of $y_{ij}$, so it is to be expected that the momentum reduces. To proceed any further, we would require the mass of each particle, and the momentum. Due to limited time, the specific details (such as angle, total momentum, particle type) of each run time in Pythia is not recorded. In this case, we have used the pion mass (139.57018 MeV) [7] , and have approximated that the total momentum is equal to the transverse momentum. The purpose of continuing with such vague assumptions is that it can still be demonstrated how the uncertainty from the tracker will affect the total uncertainty obtained from the particle flow. The pion mass was used because approximately 80% of the particles detected are pions.

The uncertainty in the Electromagnetic Calorimeter (ECAL)in Si-DET is given as:

$$\frac{u(E)}{E} = \sqrt{(\frac{0.17}{\sqrt{E}})^2 + 0.01^2} \tag{11}$$

The uncertainty in the ECAL used in ALEPH had a relative uncertainty of:

$$\frac{u(E)}{E} = \sqrt{(\frac{0.18}{\sqrt{E}})^2 + 0.009^2} \tag{12}$$

As shown in the diagram below, the improvement in uncertainty offered by the new silicon detector is negligible.

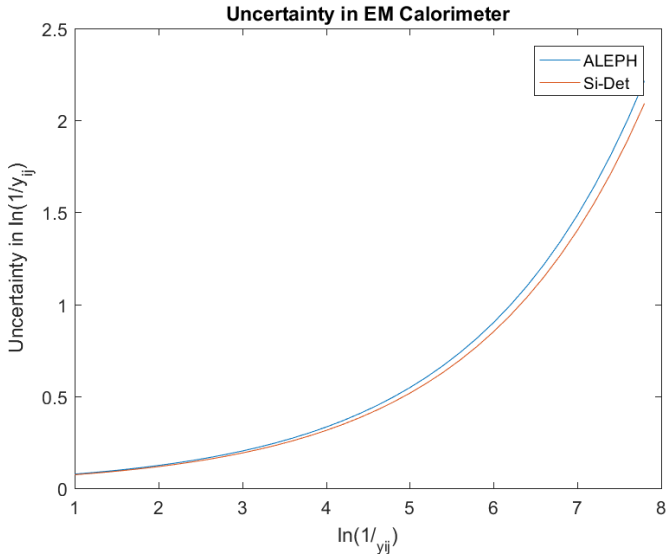


Figure 7: Uncertainty of energy in ECAL

The uncertainty in the HCAL to be used in Si-DET is given as:

$$\frac{u(E)}{E} = \sqrt{(\frac{0.55}{\sqrt{E}})^2 + 0.075^2} \tag{13}$$

The uncertainty in the HCAL used in ALEPH had a relative uncertainty of:

$$\frac{u(E)}{E} = \frac{0.85}{\sqrt{E}} \tag{14}$$

A comparison of uncertainties in the HCAL is shown below.

The compound measure is referred to as the Jet Energy resolution. For Si-DET, the jet energy resolution is:

$$\frac{u(E)}{E} = \frac{0.3}{\sqrt{E}} \tag{15}$$

The jet energy resolution of ALEPH provided by M. Dams was said to be a factor of 2 worse. The uncertainty used to smear the ALEPH data was taken

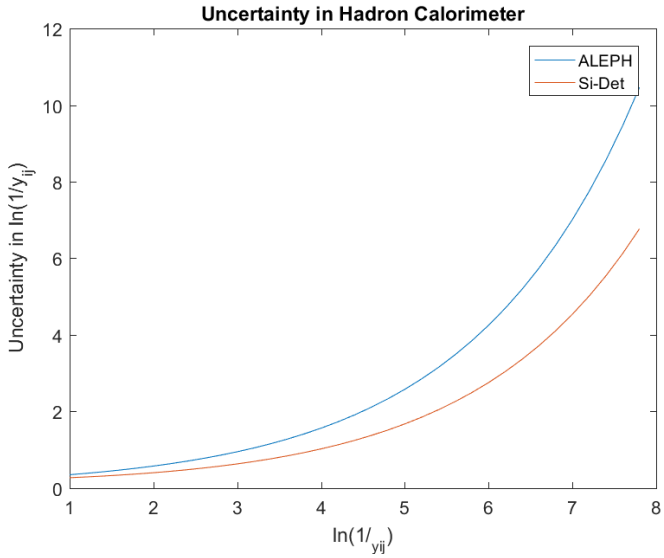


Figure 8: Uncertainty of energy in HCAL

as:

$$\frac{u(E)}{E} = \frac{0.6}{\sqrt{E}} \tag{16}$$

The jet energy resolution of ALEPH is reduced, possibly because ALEPH did not consider a concept referred to as particle flow, and may have considered each component of the detector separately. Particle flow refers to using the multiple components of the detector, and forming a combined jet. The particle event generator PYTHIA was used to simulate 100 million Z boson decays. This allows the statistical uncertainty to drop, so that an accurate representation of the proposed detectors can be made. The data that PYTHIA produced was put into a histogram, with the value of $ln(1/y_{ij})$ representing the x axis, and the y axis represents the probability of detecting a particle with an energy corresponding to $ln(1/y_{ij})$ . This is considered the 'truth distribution'. The total number of counts is denoted as $N_{tot} = \Sigma_i^N$. The probability of detecting a particle in bin i is therefore $p_i = \frac{N_i}{N_tot}$. The probability is presented per bin width.

The energy resolution for each component of the detector depends on the energy of the particles that are received. Whilst PYTHIA did generate each event one at a time, and determine the clustering energy $y_{ij}$, it did not maintain a record of the angle for each event. This is a problem, as the relationship between energy can be written as:

$$E_{min}^2 = \frac{y_{ij} \cdot E_{CM}^2}{2(1 - cos\theta_{ij})} \tag{17}$$

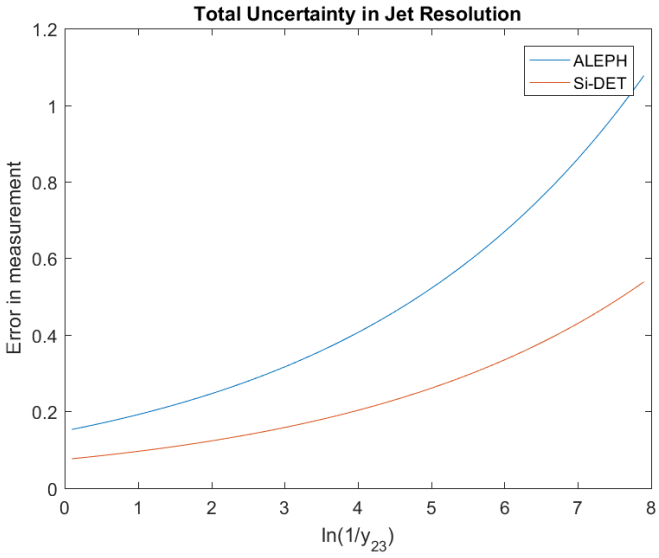


To overcome this problem, angular dependence was ignored, by substituting $\theta = 90$. This gives us the highest possible value for the energy, and therefore the highest possible value for the uncertainty in the energy. This means that the recommendation of this project will be conservative. The 'truth' distribution refers to what nature actually produces. However, there is a probability in each bin that there is a wrongful measurement so that a count in bin i originated in a neighbouring bin [8]. This can be expressed as [9]:

$$N_{measured} = \Sigma_{i=1}^{k} R(measured|truth) N_{truth} \tag{18}$$

Here, $R(measured|truth)$ represents the probability of measuring an event erroneously, and incorrectly adding a count to the wrong bin, and k represents the total number of bins. In this project, this function has been modelled as a Gaussian distribution, which inherently depends on the standard deviation (which in this case will be the measurement uncertainty). The 'truth' distribution can be recovered from the smeared distribution, if the exact causes of bin migration are known, and the significance of bin smearing is known, in a process sometimes referred to as unsmearing. The ratio $N_{smeared}/Ntruth$ is known as the correction factor, and is an important factor in unsmearing. As the correction factor increases, controlling the bin migration becomes more difficult. This is because the uncertainty in smearing, essentially the uncertainty of the uncertainty, increases.

$$\int_{\mu - w/2}^{\mu + w/2} \frac{1}{\sigma\sqrt{(2\pi)}} exp(\frac{-(x-\mu)^2}{2 \cdot \sigma^2}) dx \tag{19}$$

Where $\mu$ is the mean value, and $\sigma$ is the standard deviation. In this case, $\mu$ represents the centre of the bin, w represents the bin width, and $\sigma$ represents the uncertainty in the measurement. This tells us that the probability of bin migration depends on the uncertainty of the measurement. The effects of bin migration will also have a greater impact in sharply falling distributions. This is because there is greater variation between bins.

The bin migration matrix was set up using a diagonal algorithm. The entries on the diagonal represent the probability of correctly identifying a particle with corresponding energy in the correct bin. The entries neighbouring the diagonal represent the probability a particle being detected with a lower or higher value of $ln(1/y_{23})$. The bin migration matrix multiplies the frequency matrix, to obtain a smeared distribution. If the experimentalists bin too finely, such that the uncertainty is comparable to the bin width, the bin migration is expected to increase. The frequency distribution is calculated with millions of events. The frequency vector is divided by the total number of counts, which gives the probability of a count being in a particular bin. The frequency is also divided by the bin width, so that a dynamic bin analysis can be made.

A persistent problem in setting up the bin migration matrix is setting up the error vector. This resulted in applying a reduced uncertainty to the bin migration, causing the correction factor to be vastly reduced.

# 4 Results and Analysis

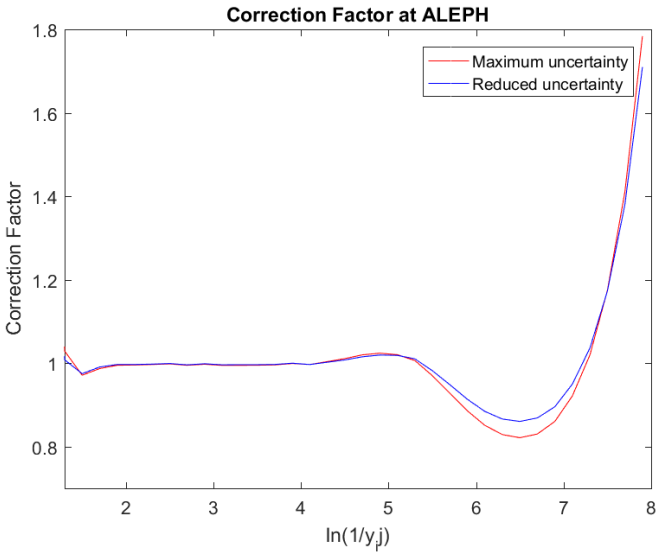


Figure 9: Comparison of correction factors with different uncertainties

Figure 8 shows the correction factors that would have been obtained at ALEPH. The red line represents the maximum uncertainty, where $\theta = 90$. The blue line represents a reduced uncertainty, where $\theta = 60$. The data that ALEPH presents is corrected for bin matrix. This means that the experimentalists believe that the bin migration is understood, and so they can apply an inverse to the smearing matrix. When applying a bin width of 0.2, and using the jet energy resolution that ALEPH had, the bin matrix is not normalized. This means that the uncertainty of the measurement is at a similar width of the bin width, so the probability of correctly identifying the bin it belongs in becomes smaller. Once $ln(1/y_{ij})$ is greater than 5, the error measurement is the same as the bin width. This is not simply an 'edge effect', where a bin matrix would only be able to migrate from one side, due to being an outer bin. Si-DET faces similar problems, but only when the value of $ln(1/y_{ij})$ is greater than 8.4. As 98% of the particle events are below 8.4, this non-normalization becomes negligible.

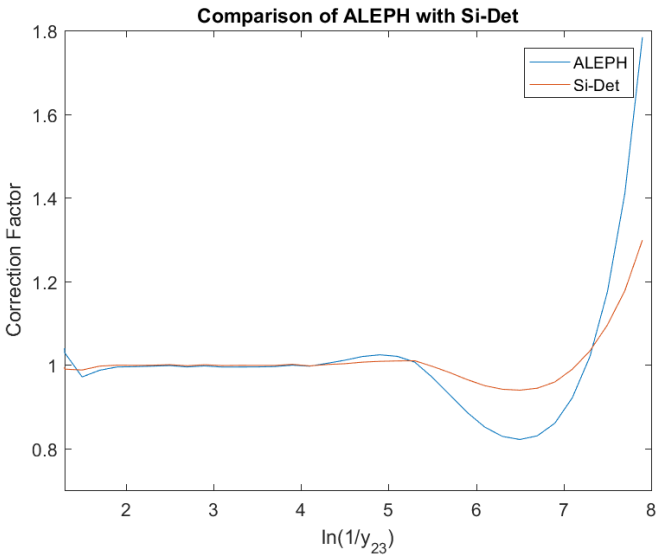


Figure 10: Comparison of correction factors between ALEPH and Si-DET

Figure 9 compares the correction factors of ALEPH with Si-DET. It is clear that the correction factor will be greatly improved with the new detector. The uncertainties will still increase as the jets become softer, but this is noticeably reduced. Referring to the minimum correction value around $ln(\frac{1}{y_{ij}}) = 6.5$, the correction factor from Si-DET appears to be 15% closer to unity.

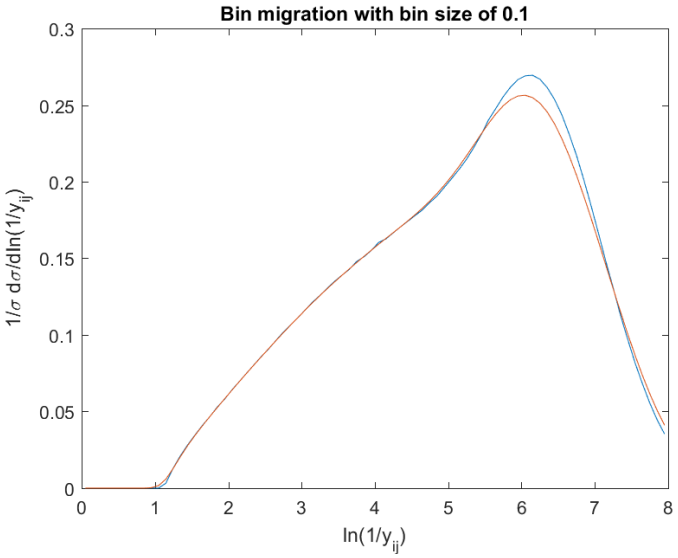


Figure 11: Bin migration of distribution with bin width of 0.1

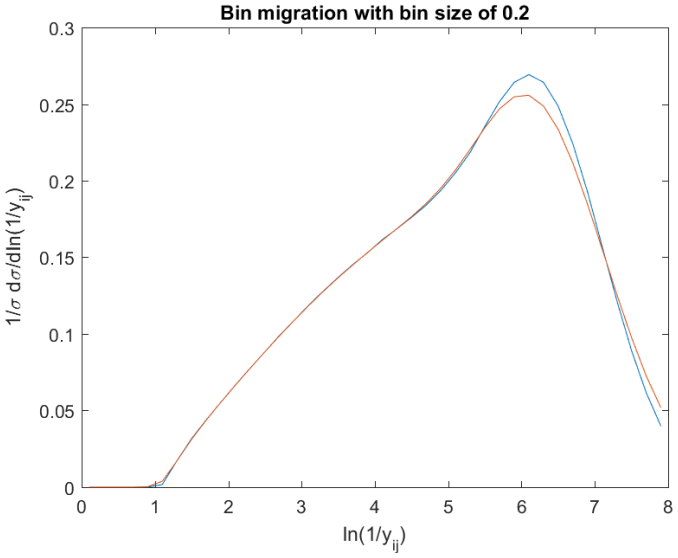


Figure 12: Bin migration of distribution with bin width of 0.2

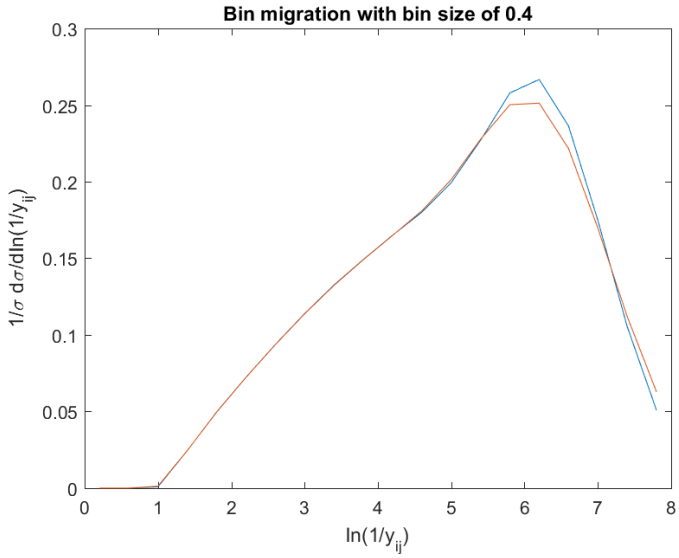


Figure 13: Bin migration of distribution with bin width of 0.4

Figures 10, 11 and 12 show the bin migration with bin widths of 0.1, 0.2, and 0.4. It should be expected that a finer binning causes a higher amount of bin migration. This is not seen, despite the bin matrix showing values that would suggest reduced smearing. This means that the values on the diagonal of the matrix were higher, which would mean that there is a greater chance of a detection correctly measured in a bin. This suggests that an error has been made.

Figure 13 shows the correction factors that arise from using different bin widths. The results show that a bin width of 0.1 has the least amount of bin smearing, which was not expected. It is interesting that there is very little difference between bin sizes of 0.2 and 0.4. These correction factors are barely distinguishable, whilst the difference of 0.1 and 0.2 is more noticeable.

Figure 15 presents the correction factor obtained from combining bin widths of 0.1 for $ln(1/y_{ij})$ between 0 and 4, and 0.2 for $ln(1/y_{ij})$ between 4 and 8. As expected from figures 13 and 14, this results in a worse correction factor than just maintaining a bin width of 0.1. Had results been reversed, this may have been an optimal binning allocation.

# 5 Discussion

With the new detectors showing a correction factor 15% less than the detectors used in ALEPH, Si-DET can provide a reduced uncertainty with the same bin width of 0.2. For softer jets, the uncertainty will still increase, but the correction factors are reduced comparing to ALEPH, so the uncertainty that will come from

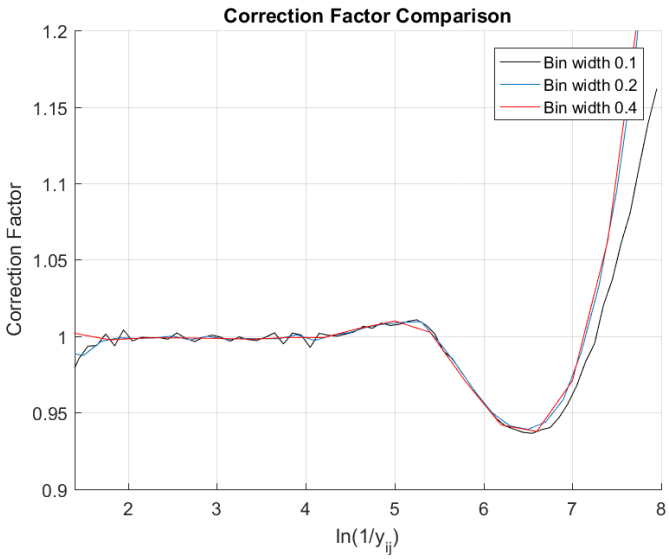


Figure 14: Correction Factors with different bin widths

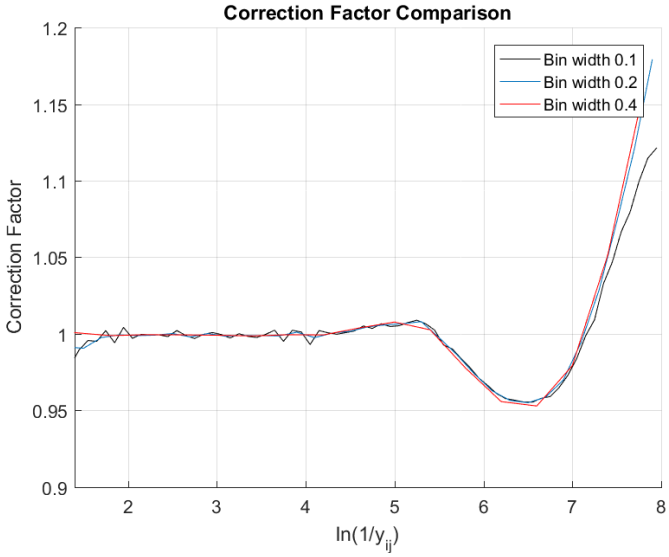


Figure 15: Correction Factor with reduced uncertainty

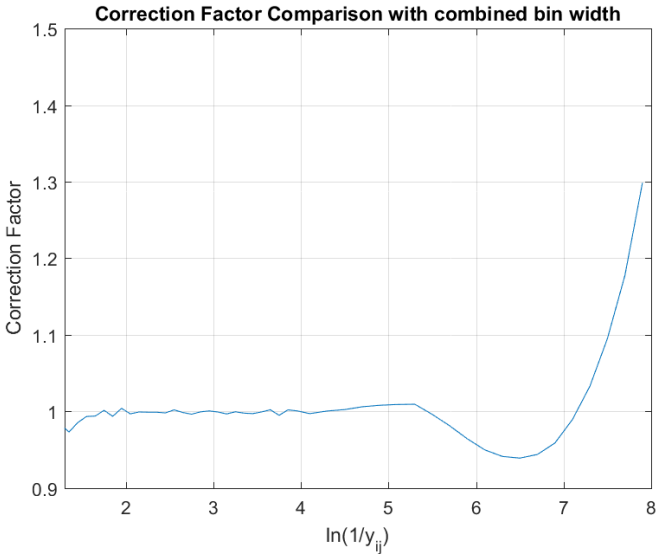


Figure 16: Correction factor that results from combined bin width of 0.1 and 0.2 presented

unsmearing the distribution will be reduced.

It is surprising that the bin migration matrix shows increased smearing with wider bins. This dubious result suggests an error in the bin migration matrix. However, inspecting the bin migration matrix, as the bin size increases, the values on the diagonal increase. This would suggest that less bin smearing is going on, despite the fact that the correction factor does not show this. If this is not an error, then one explantion could be that the sharply falling distribution is more influential in determing the correction factor than first believed. If the results are taken at face value, the smallest amount of bin migration would be a bin width of 0.1, and this would be the recommend bin width. It is interesting to note that from figure (xxxxx) that the uncertainty in $ln(\frac{1}{y_{23}}$ seems to increase past 0.2, meaning that a constant bin size of 0.2 would not account for the uncertainties of softer jets. Another factor that would help contribute to determining the maximum resolution is understanding the angular dependence. If the angle $\theta$ reduces by just 30 degrees from 90 degrees to 60 degrees, equation 15 would return an $E^2$ value twice that as before. This would cause the error to reduce by $2^{\frac{1}{4}}$, and therefore reduce the bin smearing. From the data presented, a bin width of 0.1 would be the finest resolution that could be obtained when looking for orthogonal particles to cluster. Furthermore, the mass of each particle was not recorded in PYTHIA. As the uncertainty of the particle tracker will depend on the momentum of each particle, which is related to the mass, this may have an effect. The results produced provide a basic comparison, so the effects of other parameters on bin migration can be determined.

# 6 Conclusion

The effects of bin migration were examined on a histogram distribution of the logarithmic Durham value. It was found that the proposed Silicon Detector would greatly reduce the magnitude of bin smearing. The results produced suggest a bin size of 0.1 is recommended, as this would have minimal bin smearing. This seems unlikely, and so more time would be needed to confirm these results. In any case, the resolution of Si-DET provides much reduced correction factors, which should allow future experimentalists to bin the $k\perp$ Durham jet rate as finely as ALEPH, if not finer. This is reinforced by the fact that the experimentalists at ALEPH believe they can control bin migration.

# 7 References

[1] Ellis, R.K., QCD and Collider Physics, Cambridge University Press, 1996.
[2] Salam, Gavin P. "Elements of QCD for hadron colliders." arXiv preprint arXiv:1011.5131 (2010).
[2]Heister, A., et al. "Studies of QCD at $e^+e^-$ centre-of-mass energies between 91 and 209 GeV." European Physical Journal C 35.4 (2004): 457-486. [3] Erler, Jens, et al. "Physics impact of GigaZ." Physics Letters B 486.1 (2000): 125-133.
[4] d'Enterria, David. "Physics at the FCC-ee." arXiv preprint arXiv:1602.05043 (2016).
[5] Decamp, D., et al. "ALEPH: a detector for electron-positron annihilations at LEP." Nuclear Instruments and Methods in Physics Research Section A: Accelerators, Spectrometers, Detectors and Associated Equipment 294.1 (1990): 121-178.
[6] M. Dams, Niels Bohr Institute, Copenhagen, Private Communication
[7]S. Eidelman et al. (Particle Data Group), Phys. Lett. B 592, 1 (2004) (URL: http://pdg.lbl.gov)
[8]Cowan, Glen. "A survey of unfolding methods for particle physics." Prepared for Conference on Advanced Statistical Techniques in Particle Physics, Durham, England. 2002.
[9]Mirman, Nathan E. "Study of Bin Migration in the Z Boson Rapidity Measurement at CMS." (2010).

# 8 Further Reading

[10]Quantum Chromodynamics: High Energy Experiments and Theory by Günther Dissertori, Ian G. Knowles, Michael Schmelling
[11] Skands, Peter. "Introduction to QCD." Searching for New Physics at Small and Large Scales (TASI 2012)-Proceedings of the 2012 Theoretical Advanced Study Institute in Elementary Particle Physics. Edited by Schmaltz Martin and Pierpaoli Elena. Published by World Scientific Publishing Co. Pte. Ltd., 2013. ISBN No. 9789814525220, pp. 341-420. Vol. 1. 2013.

# 9 Appendix A

To determine the uncertainty of the minimum function, an approximation of a continuous function can be used. This means that the chain rule for determining uncertainties ( equation 5) can be used to determine the error associated with it. Let

$$min(x,y) = \lim_{n\to\infty} \frac{x^n \cdot y}{x^n + y^n} + \frac{y^n \cdot x}{x^n + y^n} \tag{20}$$

or alternatively as:

$$min(x,y) = \lim_{n\to\infty} \frac{x^n \cdot y + y^n \cdot x}{x^n + y^n} \tag{21}$$

This will represent the minimum function if the limit is taken as n approaches infinity. If x is smaller than y, then $x^n + y^n \approx y^n$. The expression $\frac{x^n \cdot y}{y^n}$ will then approach zero as n approaches infinity. Likewise, we can see that $\frac{y^n \cdot x}{x^n + y^n}$ will approach x as n approaches infinity. If y is the minimum value, the exact same reasoning will show that this function will select y.

To find the uncertainty in this function, equation 4 is used. It must be noted that the limit of a derivative is equal to the derivative of a limit.

Let

$$a = \frac{x^n \cdot y + y^n \cdot x}{x^n + y^n} \tag{22}$$

Then

$$u(a) = \sqrt{\left(\frac{\partial a}{\partial x} u(x)\right)^2 + \left(\frac{\partial a}{\partial y} u(y)\right)^2} \tag{23}$$

For the sake of brevity, this derivation focuses only how uncertainty in x propagates. This gives:

$$u(a)^2 = (\frac{n \cdot x^{n-1} \cdot y + y^n x^n + y^n - n \cdot x^{n-1} x^n \cdot y + y^n \cdot x}{(x^n + y^n)^2} \cdot u(x))^2 \tag{24}$$

$$\lim_{n\to\infty} 2n - 1 = 2n, \tag{25}$$

$$\lim_{n\to\infty} n + 1 = n \tag{26}$$

$$\lim_{n\to\infty} n - 1 = n \tag{27}$$

Using the above limits, the numerator will become :

$$\frac{y^{2n} + y^n \cdot x^n}{(x^n + y^n)^2} \tag{28}$$

Now if we look at the case $x > y$, (which would imply the minimum function should not depend on x), and recall

$$\lim_{n\to\infty} x^n + y^n = x^n \tag{29}$$

we find that

$$u(min[x, y]) = (\frac{y^{2n}}{x^{2n}} + \frac{y^n}{x^n}) \cdot u(x) \tag{30}$$

Again applying the limit as n approaches infinity, note that:

$$\lim_{n\to\infty} \frac{y^n}{x^n} = 0 \tag{31}$$

This means that if x is not the minimum, then the uncertainty in the minimum function does not depend on the uncertainty of x. Now, looking at the case if $x < y$, and apply the same limits as before, we again find:

$$\frac{y^{2n} + y^n \cdot x^n}{(x^n + y^n)^2} \tag{32}$$

$$\tag{33}$$

and again use the limit:

$$\lim_{n\to\infty} x^n + y^n = y^n \tag{34}$$

which gives:

$$\frac{y^{2n} + y^n \cdot x^n}{y^{2n}} \tag{35}$$

or :

$$(1 + \frac{x^n}{y^n}) \cdot u(x) \tag{36}$$

As n approaches infinity, the second term in the brackets approaches zero, leaving us with the uncertainty in x multiplied by 1. This tells us that if x is indeed our minimum, the uncertainty of the minimum function is just the uncertainty of the smallest value.